PRP Pharmacology Research & Perspectives
Open Access

ORIGINAL ARTICLE

ADME studies of [5-^{3}H]-2′-*O*-methyluridine nucleoside in mice: a building block in siRNA therapeutics

Frederic Lozac'h, Jesper Christensen, Thomas Faller, Esther van de Kerkhof, Joel Krauser, Maxime Garnier, Karine Litherland, Alexandre Catoire, Francois Natt, Jurg Hunziker & Piet Swart

Novartis Institutes for Biomedical Research, Drug Metabolism and Pharmacokinetics, Novartis Pharma AG, Fabrikstrasse 14, 1.17, CH-4002 Basel, Switzerland

Keywords
2′-*O*-methyluridine, ADME, lithium adducts formation, mass spectrometry, QWBA, SiRNA

Correspondence
Lozac'h Frédéric, Novartis Pharma AG, Novartis Institutes for Biomedical Research, Drug Metabolism and Pharmacokinetics, Fabrikstrasse 14, 1.17, CH-4002 Basel, Switzerland. Tel: +41 61 69 68 516; Fax: +41 61 69 68 582
E-mail: frederic.lozach@novartis.com

Funding Information
No funding information provided.

Received: 11 September 2015; Accepted: 7 December 2015

Pharma Res Per, 4(1), 2016, e00209, doi: 10.1002/prp2.209

doi: 10.1002/prp2.209

Abstract

The chemical modification 2′-*O*-methyl of nucleosides is often used to increase siRNA stability towards nuclease activities. However, the metabolic fate of modified nucleosides remains unclear. Therefore, the aim of this study was to determine the mass balance, pharmacokinetic, and absorption, distribution, metabolism, and excretion (ADME)-properties of tritium-labeled 2′-*O*-methyluridine, following a single intravenous dose to male CD-1 mice. The single intravenous administration of [5-^{3}H]-2′-*O*-methyluridine was well tolerated in mice. Radioactivity was rapidly and widely distributed throughout the body and remained detectable in all tissues investigated throughout the observation period of 48 h. After an initial rapid decline, blood concentrations of total radiolabeled components declined at a much slower rate. [^{3}H]-2′-*O*-Methyluridine represented a minor component of the radioactivity in plasma (5.89% of [^{3}H]-$AUC_{0\text{-}48\ h}$). Three [^{3}H]-2′-*O*-methyluridine metabolites namely uridine (M1), cytidine (M2), and uracil (M3) were the major circulating components representing 32.8%, 8.11%, and 23.6% of radioactivity area under the curve, respectively. The highest concentrations of total radiolabeled components and exposures were observed in kidney, spleen, pineal body, and lymph nodes. The mass balance, which is the sum of external recovery of radioactivity in excreta and remaining radioactivity in carcass and cage wash, was complete. Renal excretion accounted for about 52.7% of the dose with direct renal excretion of the parent in combination with metabolism to the endogenous compounds cytidine, uracil, cytosine, and cytidine.

Abbreviations

2′OMeU, 2′-*O*-methyluridine; ADME, absorption, distribution, metabolism, and excretion; AUC, area under the curve; Cmax, apparent maximum concentration; CTP, cytidine triphosphate; M, metabolite; nd, not detected; p.d., postdose; QWBA, quantitative whole-body autoradiography; RNAi, RNA interference; siRNA, short interfering RNA; Tmax, time at which Cmax is observed; UMP, uridine monophosphate; UTP, uridine triphosphate.

Introduction

To increase the "drug-like" properties of short interfering RNA (siRNAs), these biomolecules are often chemically modified. RNA is known to be less stable than DNA as the 2′-OH group in RNA promotes RNA hydrolysis under acidic and basic conditions (Rana 2007). Chemical modifications of siRNAs can provide desired properties, such as increased thermodynamic stability and/or stability towards nuclease degradation, the latter which can lead to increased half-life. Morrissey et al. (2005) reported an improved plasma elimination half-life in mice from 2 to 49 min by comparing an unmodified siRNA versus the chemically stabilized version.

The insertion of chemical modifications is also an important strategy to improve RNA interference (RNAi) and reduce off-target effects such as off-target silencing and immunostimulation (Singh et al. 2011). Several chemical modifications of siRNAs exist (Behlke 2008; Watts et al. 2008; Shukla et al. 2010; Bramsen and Kjems 2011; Engels 2013) and sugar modifications are the most widely used siRNA modifications compared to backbone and base modifications. These chemically modified siRNAs were shown to be well tolerated and to also protect against endonuclease activities. However, with the passenger strand being more susceptible to modification than the guide strand, stability is more dependent on the location of the modification within the siRNA.

The 2′-position can indirectly improve nuclease resistance of the internucleotide phosphate bond and can at the same time increase duplex stability. This position may furthermore provide protection from immune activation. The 2′-position modifications have been extensively investigated, as the 2′-OH group is not needed for the activity of siRNAs (Chiu and Rana 2003). Incorporation of 2′-*O*-methyl (2′OMe) has the following positive consequences: (1) full retainment of potency (2) extended stability in serum (3) well tolerated in siRNAs, by lowering the risk towards activation of the innate immune system (Watts et al. 2008; Castanotto and Rossi 2009; Whitehead et al. 2009). The precise location of incorporation is important, and RNAs that are entirely substituted with 2′OMe are inactive (Behlke 2006). Despite the stabilizing effect provided by the 2′OMe nucleosides, the siRNA can still be degraded in vivo. We recently showed that the 2′OMe-modified [^{3}H]-siRNA was rapidly and completely degraded (Christensen et al. 2013).

The 2′-fluoro (2′F) modification is also an alternative modification that has been studied for safety in rodents with a reported No Observable Adverse Effect Levels (NAOELs) of 500 mg/kg per day (Richardson et al. 1999). For the biosynthesis of DNA and RNA, the precursor triphosphate nucleotides can either originate from biosynthesis of nucleotides (the de novo pathway) or from recycling of nucleotides (the salvage pathway). Subsequently, nucleosides are phosphorylated by kinases to mono-, di- and triphosphate nucleotides. Nucleoside analogs were found to be incorporated into DNA and RNA. For several of these nucleoside analogues, toxicity has also been implicated or correlated with nuclear and/or mitochondrial DNA incorporation (Richardson et al. 2002). Nevertheless, the ability of nucleoside analogs to be incorporated into DNA/RNA (impairing their synthesis) has been utilized for viral and cancer therapeutics. Even though the 2′OMe-modified nucleoside is an endogenous compound in humans (Smith and Steitz 1997; Werner et al. 2011), the ability of this nucleoside analog to participate in the salvage biosynthesis of RNA remains unknown.

The aim of this study was to determine the absorption, distribution, metabolism, and excretion (ADME)-properties of [^{3}H]-2′-*O*-methyluridine following intravenous administration to mice, in support of the preclinical safety studies and clinical development of siRNA therapeutics.

Materials and Methods

Test compound and radiolabeling of nucleoside

The ADME-properties of 2′-*O*-methyluridine were studied in mice. The modified nucleoside was synthesized and radiolabeled with tritium following procedures previously described (Christensen et al. 2012). The tritium atom was incorporated into the chemically stable C5-position. The radiochemical purity was 89% by Reverse Phase - High Pressure Liquid Chromatography (RP-HPLC).

In vivo experiments

The animal studies were approved by Animal Care and Use Committees of the Kanton Basel, Switzerland. Male albino CD-1 mice (Charles River, France Saint-Germain sur l'Arbresle, 30–36 g, 8–10 weeks) received an intravenous bolus injection in the *vena saphena* of 1 mg/kg [5-^{3}H]-2′-*O*-methyluridine in 0.9% sodium chloride under a light inhalation anesthesia by isoflurane. The dose volume was 2 mL/kg, and the total amount of radioactivity administered was 53–67 MBq/kg. The specific radioactivity was 50 MBq/mg.

For blood and plasma pharmacokinetics of total radioactivity and metabolite profiling, eight mice were dosed to cover the pharmacokinetics time course of 48 h. From each animal two blood samples were taken; one blood sample between dosing and termination, and the second blood sample with tissues were harvested at the respective terminal time points. This sampling procedure allowed us to pool sufficient material at each time point for total radioactivity detection and the generation of radiochromatograms.

Blood was collected from either *vena saphena* (opposite leg than used for dosing) or *vena cava* (for end-points) in EDTA containing tubes at 0.083, 0.5, 1, 2, 4, 8, 24, and 48 h postdose. A blood aliquot was processed immediately to plasma by centrifugation at 3000 *g* for 10 min at 4°C. From each blood and plasma sample, an aliquot was processed for determination of radioactivity. A second aliquot was dried at 37°C to evaporate tritiated water in a drying oven before the processing for radiometry by Liquid Scintillation Counter (LSC). For ach time point, tissues samples of the liver, lung, kidney, heart, spleen,

salivary glands, and small intestine were collected and together with the remaining blood and plasma samples snap frozen and stored at −80°C until further analysis. Quantitative whole-body autoradiography (QWBA) was performed at 0.167, 1, 2, 24, and 48 h postdose.

Two animals were housed in metabolic cages up to 48 h for urine and feces collection allowing determination of the route of excretion and the mass balance.

Analytical methods

Radiometric analysis

Radioactive signals in the different matrices were quantified by LSC, using Liquid Scintillation Systems 2500 TR from Packard Instr. Co. (Meriden, CT). For quench correction, an external standard ratio method was used. Quench correction curves were established by means of sealed standards (Packard). Background values were prepared for each batch of samples according to the respective matrix. The limit of detection was defined as 1.8 times the background value. All determinations of radioactivity were conducted in weighed and nondried/dried samples. Measured radioactivity for blood, plasma, and tissues was converted into concentrations (mol equivalents per volume or gram) considering the specific radioactivity and assuming a matrix density of 1 g/mL.

Tritiated water

The determination of tritiated water was based on urine measurements. Urine was processed and analyzed in two different ways: (1) An aliquot (50 μL) of each urine sample was collected and total nondried radioactivity determined. (2) Another aliquot (50 μL) of each urine sample was dried at 37°C and the pellet collected, the latter was used for the determination of total dried radioactivity. The formation of tritiated water was calculated according to Tse and Jaffe (1991). In brief: the biologic stability of ^{3}H-labels can be estimated by the extent of tritiated water formation in urine, and by assuming that equilibrium was reached between urine and body water. The determined radioactivity (dpm/mL) for each urine sample was extrapolated from the midpoint of the collection interval to zero time, based on the known half-life of water of 27.1 h in mice (Richmond et al. 1962). The percentage of the radioactive dose that was transformed to tritiated water was calculated by multiplying the concentration of tritiated water at time zero with the exchangeable body water 72.5% of body weight of the mouse (Davies and Morris 1993), and dividing the product by the radioactive dose. For each calculation, the change in the body weight during the experiment was not considered.

Quantitative whole-body autoradiography

Mice were killed by deep isoflurane inhalation. After deep anesthesia, blood for radioactivity determination by LSC was collected by *vena saphena* (the other leg than the one used for dosing). The animals were then submerged in n-hexane/dry ice at −70°C for approximately 30 min. The carcasses were stored at −18°C and all subsequent procedures were performed at temperatures below −20°C to minimize diffusion of radiolabeled materials into thawed tissues. Sections were prepared as follows: in brief, 40 μm thick lengthwise dehydrated whole-body sections were prepared and exposed to Fuji BAS III imaging plates (Fuji Photo Film Co., Ltd., Tokyo, Japan) in a lead-shielded box at room temperature for 2 weeks, and then scanned in a Fuji BAS 5000 phosphor imager (Fuji Photo Film) at a 50 μm scanning step. The concentrations of total radiolabeled components in the tissues were determined by comparative densitometry and digital analysis of the autoradiogram; blood samples of known concentrations of total radiolabeled components processed under the same conditions were used as calibrators.

Structural elucidation of nucleoside metabolites

The structural characterizations of the parent and metabolites in plasma, excreta, and the various tissues were performed by LC–MS (and/or Liquid Chromatography Mass Spectrometer (LC–MS^2)) and/or Nuclear Magnetic Resonance (NMR) analysis. A reverse phase Ultra High Pressure Liquid Chromatography (UHPLC) method was used for profiling of parent and metabolites. Mass spectrometric data were obtained using LTQ-Orbitrap (ThermoFisher Scientific, Bremen, Germany) (technology 1), or a Synapt G2-S quadrupole time of flight (Waters) (technology 2) in electrospray negative or positive mode. The radiochromatogram profiles were analyzed and identified with off-line radioactivity analysis. Metabolites were identified in each profile by MS and/or corresponding peaks in the radiochromatogram *versus* a control sample. Electrospray ionization of [5-^{3}H]-2′-*O*-methyluridine and its metabolites in the positive ion, using technology 1, mode resulted predominantly in $[M+H]^+$ ions. Samples were analyzed in the full-scan MS mode for acquisition of the $[M+H]^+$ molecular ion data in the positive ion mode ($[M-H]^-$ in the negative mode). The high resolution and accurate mass capabilities of the instrument allowed for metabolite elemental compositions to be determined from the molecular ion data. For the acquisition of fragmentation data for metabolite structural elucidation, selected samples were analyzed by MS/MS using CID (Collision Induced Dissociation). Data-dependent triggering which was based on a list of molecular ion masses for known or suspected metabolites, was used to

select precursor masses for subsequent MS/MS scans, allowing for fragmentation spectra for multiple metabolites to be acquired in a single run. Full mass spectra were acquired for the parent compound and each metabolite. Electrospray ionization used in the scope of the technology 2, resulted nearly only in $[M+Na]^+$ molecular ions. A postcolumn addition of methanol containing lithium chloride was applied to enhance the $[M+H]^+$ and $[M+Li]^+$ versus $[M+Na]^+$ adducts formation. Generated data were stripped based on the mass difference $[M+Li]^+$ versus $[M+H]^+$ to clean the acquired full-scan mass spectrum. Further analysis as retention time and MS/MS mass spectra comparison with authentic standards or hydrogen/deuterium (H/D) exchange experiments were also performed. For H/D experiments the water and methanol in the mobile phases were replaced by D_2O or MeOD, respectively.

Sample preparation of matrices for metabolite profiling

For metabolite profiling of plasma, the two collected plasma samples per time point were pooled and extracted with two volumes of acetonitrile (100 μL) to allow protein precipitation. The mixtures were vortexed and centrifuged with an acceleration of 17500 *g* for 15 min at 4°C (Beckman, Brea, CA, United States, GS-15R). To reduce the volume to approximately 20 μL, the supernatants were then concentrated under a nitrogen flow. For metabolic profiling of urine, each sample was centrifuged (as described for plasma), and the supernatant was used for analysis. Feces was homogenized and extracted with two volumes of acetonitrile (400 μL). The mixture was vortexed and centrifuged (as described for plasma). The supernatant was then concentrated under a nitrogen flow to reduce the volume to approximately 50 μL. Selected tissues showing relative high exposures of radioactivity in the QWBA, were homogenized with 4 volumes of water. The homogenates were extracted with 2 volumes of acetonitrile, vortexed, and centrifuged (as described for plasma). The pellet was dissolved in 200 μL water and sonicated for 30 min, 400 μL acetonitrile was then added, and the sample was kept at −20°C overnight. The mixture was then centrifuged (as described for plasma). The two supernatants were combined and concentrated under a nitrogen flow to approximately 200 μL. 20 μL sample was diluted with 50 μL water before analysis. Extraction recoveries of radioactivity in the supernatants for all matrices were generally in excess of 85%.

Sample preparation of tissues for NMR analysis

Selected tissues (kidney, liver, salivary gland, small intestine, and spleen) from the 1 h postdosing time point were combined, homogenized, extracted, and concentrated under a nitrogen flow. The sample was injected on a UHPLC system, and the effluent was fractionated according to time, in order to isolate metabolites for NMR structure identification (600 MHz Bruker instrument).

UHPLC-MS-RA metabolite identification of metabolites (technology 1)

Selected plasma, excreta, and tissue samples were analyzed for metabolite identification by UHPLC-MS-RA following procedures previously described (Christensen et al. 2013). In addition, MS^2 was acquired with a multiple RF amplitude of 500.00 V and the following CID parameters; isolation width of 1.0 m/z; normalized collision energy at 35.0 V; actualization Q 0.25 and activation time 30.00 msec.

UHPLC-MS-RA metabolite identification of metabolites (technology 2)

Selected plasma, urine, and tissue samples were analyzed for metabolite identification by UHPLC-MS-RA. Separation was accomplished using a UHPLC system from Waters (Milford, MA), Acquity system equipped with two binary pumps including a degasser, an autosampler, and a column oven. The operating software monitoring the UHPLC system was Masslynx™ version 4.1 SCN883 (Waters, Milford, MA, United States). Between 10 and 100 μL sample was injected on a reverse phase C18 column (Waters Acquity UPLC HSS T3; 150 × 2.1 mm; 1.7 μm particles) with a guard Waters Acquity UPLC HSS column attached (5 × 2.1 mm; 1.7 μm particles). The column was maintained at 30°C, and the flow rate was 0.35 mL/min. The components were eluted with a gradient of mobile phase A (10 mmol/L ammonium formate (pH adjusted to 3) versus mobile phase B (0.1% [vol/vol] formic acid in methanol). Mobile phase B was maintained at 0% from 0 to 2 min, increased to 20% at 10 min, increased to 95% at 12 min, and maintained at 95% from 12 to 15 min. After elution from the column, the effluent was mixed with a make-up flow composed of 0.1 up to 0.3 mL/min of methanol or methanol containing lithium chloride (Acquity binary pump) to first increase the droplets per well during fraction collection and second produce some lithium adducts in a same magnitude as protonated molecule during mass measurements. The effluent was then split for MS and fraction collection (Gilson GX-271 operation software was Trilution LC, Gilson S.A.S, Villiers le Bel, France) into 96-well LumaPlates (6 sec fraction size). Mass measurements were made online using a Q-ToF Synapt G2-S mass spectrometer (Waters) operating under Masslynx™, version 4.1 SCN883

for instrument control, data acquisition, and data processing. From 1.5 to 15 min, the mass spectrometer was set to scan in ESI positive or negative mode with resolution set at 20,000 and a *m*/*z* window from 50 to 600. Mass spectra were obtained using a capillary voltage of ESI$^+$/ESI$^-$ 2.0/2.5 kV, a desolvatation gas flow of ESI$^+$/ESI$^-$ 500/800 (L/H), a source temperature at ESI$^+$/ESI$^-$ 100/120°C, a sampling cone of 40 V and a source offset of 80. A solution of leucine enkephalin was infused through the reference channel of the LockSpray interface to generate lock-mass signals for obtaining accurate mass data.

Pharmacokinetic analysis

Pharmacokinetic parameters were calculated using Phoenix™ WinNonlin® software (version 6.1.0.173; Pharsight Corp., Mountain View, CA). The pharmacokinetic estimations were based on a noncompartmental analysis model. The tissue to blood C_{max} and AUC_{last} ratios were determined when possible. The AUC_{last} values were calculated using the linear trapezoidal rule. For metabolite profiles, the peaks in the radiochromatograms were integrated, and from the relative peak areas, the concentrations of individual radiolabeled components in plasma/serum, and the amounts of individual radiolabeled components in excreta were calculated as follows:

$$C_{i,plasma} = C_{RA,plasma} \times \frac{R_{SP}}{100\%} \times \frac{RPA_i}{100\%} \quad \text{and}$$

$$A_{i,excreta} = C_{RA,excreta} \times \frac{R_{SP}}{100\%} \times \frac{RPA_i}{100\%}.$$

With: $C_{i,plasma}$ Molar concentration of radiolabeled component i in plasma/serum; $C_{RA,plasma}$ Molar concentration of total radiolabeled components (radioactivity) in plasma; R_{SP} Recovery of radioactivity after sample preparation (%); RPA_i Relative peak area of radiolabeled component i in radiochromatogram (% of total area under the radiochromatogram); $A_{i,excreta}$ Amount of radiolabeled component i in excreta (urine or feces; % of dose); $C_{RA,excreta}$ Amount of total radiolabeled components (radioactivity) in excreta (urine or feces; % of dose).

Results

Blood/plasma pharmacokinetics of total radiolabeled components

After i.v. dosing of [5-^{3}H]-2′-*O*-methyluridine, the concentrations of total radiolabeled components were measurable throughout the 48-h observation period in dried blood and plasma (Fig. 1). The concentration of total radiolabeled components declined in a multi-exponential manner in both matrices. Following the apparent C_{max} at 5 min, the total radioactivity declined rapidly to 1-h postdose, and a slower elimination rate occurred from 4-h postdose onwards with Tlast at 48 h and an estimate of the terminal elimination half-life of 21.4 h for dried plasma. In all cases, samples dried prior to radioactivity analysis showed lower levels of total radioactivity suggesting the formation of tritiated water.

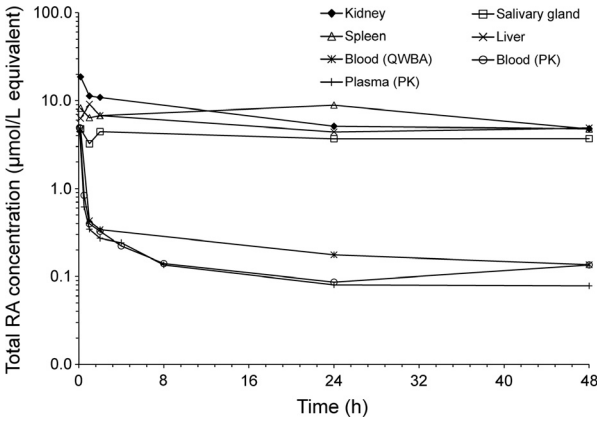

Figure 1. Individual concentration time cources of total radiolabeled components (RA) in dried plasma, blood by liquid scintillation counting and selected tissues by quantitative QWBA following a single intravenous (i.v.) dose of 1 mg/kg [5-^{3}H]-2′-*O*-methyluridine to male CD1 mice (n = 1 per time point).

In plasma, the 2′-*O*-methyluridine concentrations were derived for the metabolite patterns. 2′-*O*-methyluridine was detectable up to 24 h after dosing in plasma (Fig. 2). Following the apparent C_{max} at 5 min (0.402 nmol/L equivalents), a rapid decline from 5 min to 1-h postdose followed by a slower decline from 4-h postdose onwards with associated half-life of 4.98 h was observed. The $AUC_{0\text{-}48h}$ ratio's of total radioacitivity over parent compound was about 17 and the plasma clearance of 2′-*O*-methyluridine was estimated to be higher than the liver blood flow and amounting to 157 mL/min × kg. This result indicates that parent compound was a minor component of the total radioactivity in dried plasma and that the compound undergoes extrahepatic metabolism.

Tissue distribution and mass balance

Following single intravenous administration of [5-^{3}H]-2′-*O*-methyluridine, the total radiolabeled components were rapidly and widely distributed throughout the body. At the last time point of 48 h, all investigated tissues including blood contained measurable amounts of radioactivity. T_{max} was observed in most matrices at the first sampling point (10 min p.d.) or at 1 or 2 h after administration. However, in adrenal (medulla),

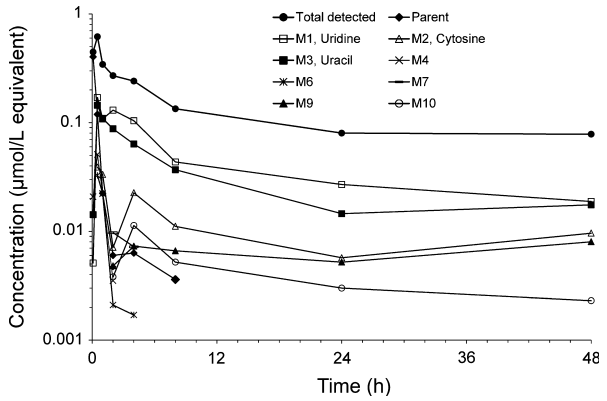

Figure 2. Parent [5-^{3}H]-2′-*O*-methyluridine and metabolites in plasma, following a single i.v. administration (nominal dose 1 mg/kg). Total detected represents total radiolabeled components in dried plasma (n = 1 per time point). Concentrations (μmol/L equivalent) are based on radioactivity peaks measured by TopCount in the respective plasma radiochromatograms per time point and the specific radioactivity.

bone marrow, fat (brown), and spleen, T_{max} was observed at distinctly later time points (24 or 48 h p.d.). The highest concentrations of total radiolabeled components (C_{max} values) were observed in the kidney and its substructures, which were 2.6- to 8.8-fold higher than in blood (4.73 nmol/g). Additionally, high concentrations of total radiolabeled components were determined in spleen (red and white pulp) and pineal body, as being 2.0- to 2.2-fold higher than in blood, respectively. In other matrices, the C_{max} tissue over blood ratio was smaller than 2. Total radiolabeled components were detectable in the brain up to 48 h p.d. Overall, the highest exposures of total radiolabeled components, based on the AUC_{last} values, were observed in the kidney (cortico-medulla junction and cortex), lymph nodes, and spleen (red and white pulp), being 27- to 36-fold higher than in blood (13.0 h × nmol/g). In summary, the AUC_{last} values in more than 90% of the matrices were greater than that of blood. Figure 1 displays concentration-time profiles of total radiolabeled components in dried blood, dried plasma, the liver, lung, kidney, heart, spleen, salivary glands, and small intestine after [5-^{3}H]-2′-*O*-methyluridine administration, and Figure 3 displays selected whole-body autoradioluminograms.

Mass balance data obtained for [^{3}H]-2′-*O*-methyluridine at 48 h showed that 52.7% of the radioactive dose was excreted via the urine, 2.34% of the dose was recovered in the feces, and that 38.6% of the radioactivity was still in the carcass. About 8.67% of radioactivity was converted to tritiated water, resulting in an overall recovery of radioacitivity of 102.3%.

Metabolite identification

Following i.v. dosing of [5-^{3}H]-2′-*O*-methyluridine ten metabolites were observed in plasma (Table 1), excreta (Table 2), and tissues Table 3) (M1–M10). However, six metabolites could not be identified by MS analysis, their structures thereby remaining unknown.

Based on the metabolite structures, the proposed metabolic pathways in the mouse are shown in Figure 4. The order of the metabolic reactions leading to the metabolites of second- and higher generation is not known. [^{3}H]-2′-*O*-methyluridine was metabolized by two main reaction types: *O*-demethylation (M1) and *N*-dealkylation (M3).

Metabolite profiles in plasma, excreta, and tissues

Plasma

Plasma samples up to 48 h postdosing were prepared for LC-MS-RA analysis, and metabolite profiles were processed (Fig. 5A). The kinetic profiles of parent 2′-*O*-methyluridine and metabolites are illustrated in Figure 2. [5-^{3}H]-2′*O*-methyluridine accounted for only 5.89% of the $AUC_{0\text{-}48h}$ of the total radiolabeled components (fourth most abundant). The major contributors were the *O*-demethylated product M1 (uridine, T_{max} 30 min *p.d.*), M3 (uracil, T_{max} 30 min p.d.), and M2 (cytosine) accounting for 32.8%, 23.6%, and 8.11% of the total radioactivity plasma AUC, respectively (Table 1). Other metabolites as M4, M6, M7, M8, M9, and M10 (which were not characterized) ,and M5 (cytidine) were considered as minor (accounting for between 1.12% and 5.21% of the $AUC_{0\text{-}48h}$ of the total radiolabeled components). Estimated apparent terminal elimination half-lives for uridine, cytosine, and uracil amounted to 12.2 h, 20.3 h, and 10.0 h, respectively, and were close to available data in the literature (Rasenack et al. 1978).

Excreta

Urine fractions from the 0 to 48 h interval contained around 52.7% (including 6.81% cage wash) of the administered radioactivity (Table 3, Fig. 5B). The [5-^{3}H]-2′*O*-methyluridine accounted for the most of the radioactivity in the urine (31.2% of dose), other metabolites as M1 (uridine), M2 (cytosine), M3 (uracil), M4, and M5 (cytidine) were detected in a range between 0.0771% and 4.11%.

Feces metabolite profiles represented only 2.34% of the administered radioactivity (Table 3, Fig. 5B). All detected metabolites were present in traces. Among these metabolites, [5-^{3}H]-2′*O*-methyluridine was the most prominent

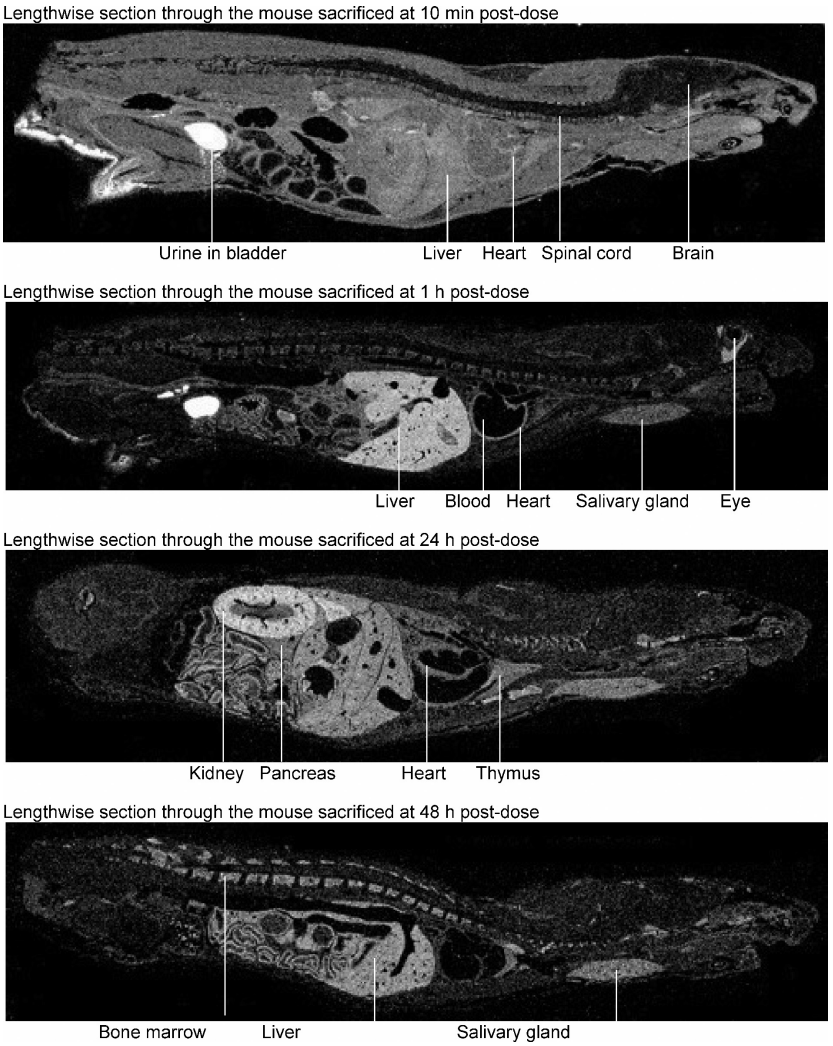

Figure 3. Selected whole-body autoradioluminographs at 10 min and at 1, 24, and 48 h after a single intravenous dose of 1 mg/kg [5-^{3}H]-2′-*O*-methyluridine to male CD-1 mice. The whitest area corresponds to the highest concentration of total radiolabeled components.

but represented only 0. 489% of the administered radioactive dose. In total, during the 0–48 h time intervals, for urine and feces, together, metabolites accounted for ~9% of the dose recovered in excreta.

Tissues

From the 1-h time point after *i.v.* administration of [5-^{3}H]-2′-*O*-methyluridine, the following tissues were analyzed: Heart, kidney, liver, lung, salivary gland, small intestine, and spleen. The results are summarized in Table 3, and metabolite profiles are shown Figure 5C. The metabolites, uridine (M1) and uracil (M3) were the most significant radiolabeled compounds observed in those tissues. The parent compound was only observed as a minor component in the small intestine (without content, 2.78% of total radioactivity). Uridine and uracil were the most abundant radioactive components observed in heart (28.4% and 46.6% of total radioactivity, respectively), liver (47.6% and 28.8% of total radioactivity, respectively), and spleen (32.9% and 57.9% of total radioactivity, respectively). The uracil metabolite was the most abundant radioactive component observed in kidney (89.4% of total radioactivity), lung (83.4% of total radioactivity), salivary gland (90.9% of total radioactivity), and small intestine (67.8% of total radioactivity).

Discussion

The ADME-properties of [^{3}H]-2′-*O*-methyluridine in the mouse were investigated in order to understand the bio-

Table 1. Concentrations and AUC0–48 h values of radiolabeled components in plasma of male CD1 mice following a single iv dose of 1 mg/kg [5-^{3}H]-2′*O*-methyluridine, pool of 2 mice. The data are based on metabolites profiles.

	Concentration (μmol/L)								AUC0-48 h	
Time (h)	0.083	0.5	1	2	4	8	24	48	(h·μmol/L)	(% AUC of total RA)
M1, uridine	0.0051	0.170	0.108	0.1301	0.104	0.0434	0.0269	0.0188	1.87	32.8
M2, cytosine	n.d.	0.0389	0.0333	0.0071	0.0226	0.0111	0.0057	0.0096	0.461	8.11
M3, uracil	0.0142	0.144	0.1093	0.0875	0.0635	0.0368	0.0145	0.0175	1.34	23.6
M4	0.0208	0.0509	0.0221	0.0035	–	–	–	0.0000	0.0503	0.88
M5, cytidine	–	0.044	–	0.0086	0.0103	–	–	0.0000	0.0639	1.12
M6	–	0.0326	0.0223	0.0021	0.0017	–	–	0.0000	0.0400	0.70
M7	–	–	–	0.0097	0.0072	–	–	0.0000	0.0362	0.64
M8	–	–	–	0.0047	–	–	–	0.0000	0.0071	0.12
M9	–	–	–	0.0048	0.0073	0.0066	0.0052	0.0080	0.296	5.21
M10	–	–	–	0.0038	0.0113	0.0052	0.0030	0.0023	0.179	3.14
2′*O*-methyluridine	0.402	0.119	0.0223	0.0060	0.0063	0.0036	–	0.0067	0.335	5.89
Sum of additional components	0.0037	0.0177	0.0259	0.0027	0.0065	0.0279	0.0248	0.0152	1.01	17.8
Total detected	0.446	0.617	0.343	0.270	0.241	0.134	0.080	0.0781	5.69	100

–, not detectable.

Table 2. Amounts of radiolabeled components in excreta of male CD1 mice following a single is dose of 1 mg/kg [5-^{3}H]-2′*O*-methyluridine. Percent of dose for the metabolites is based on metabolite profiles in urine and feces, (average of $n = 2$).

Time (h)	Urine (0–48 h) (% of RA dose)	Feces (0–48) (% of RA dose)	Total excretion (% of RA dose)	Cage wash (0–48) (% of RA dose)	Carcass 48 h (% of RA dose)	Calculated ^3H_2O (% of RA dose)
M1, uridine	0.156	–	0.156			
M2, cytosine	0.0771	–	0.0771			
M3, uracil	3.61	0.418	4.03			
M4	4.11	0.191	4.30			
M5, cytidine	1.83	0.102	1.94			
M6	0.265	0.0502	0.315			
M10	0.0931	–	0.0931			
2′*O*-methyluridine	31.2	0.489	31.7			
Sum of additional components	4.56	1.09	5.66			
Total detected	45.9	2.34	48.3	6.81	38.6	8.67

–, not detectable.

Table 3. Amounts of radiolabeled components 1 h *p.d.* in selected tissues of male CD1 mice following a single is dose of 1 mg/kg [5-^{3}H]-2′*O*-methyluridine. Percent of dose for the metabolites is based on metabolite profiles in the respective issue.

Metabolite	Heart (%)	Kidney (%)	Liver (%)	Lung (%)	Salivary gland (%)	Small intestine (%)	Spleen (%)
2′*O*-methyluridine	–	–	–	–	–	2.78	–
M1, Uridine	28.4	10.6	47.6	2.31	6.88	3.10	32.9
M2, Cytosine	6.81	nd	17.8	2.41	–	–	3.62
M3, Uracil	46.6	89.4	28.8	83.4	90.9	67.8	57.9
M4	–	–	–	–	–	2.35	–
M7	2.28	–	–	–	–	–	5.54
P4.5	15.9	–	–	–	–	22.1	–

–, not detectable.

logical impact of this nucleoside in a siRNA sequence and to support preclinical safety studies and clinical development of siRNA therapeutics.

Following intravenous administration of [5-^{3}H]-2′-*O*-methyluridine, the parent compound could be determined in plasma up to 24 h (by LC-MS-RA) and was eliminated

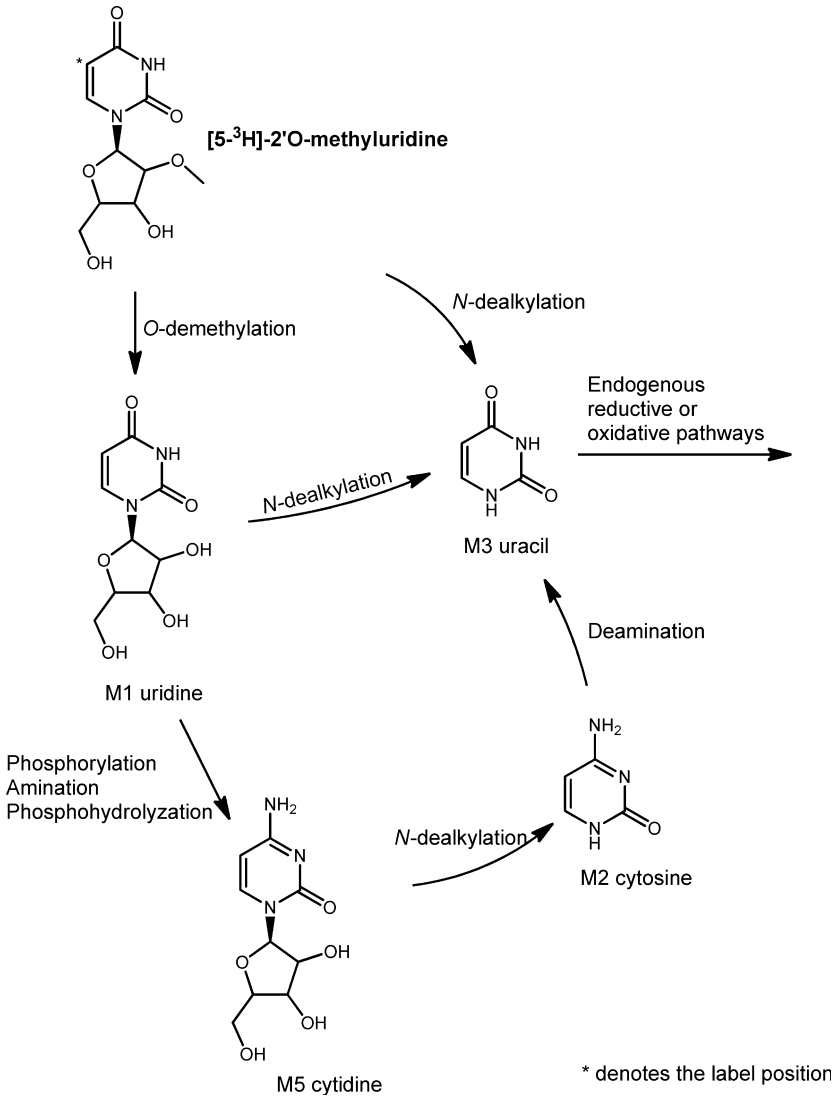

Figure 4. Proposed metabolic pathways of 2′-*O*-methyluridine in the mouse.

with a half-life of about 5 h. After an initial rapid decline of total radiolabeled components, blood concentrations declined slowly and were measurable throughout the observation period of 48 h in blood and plasma. Measurements of total radioactivity in dried blood were comparable with results derived from the QWBA data (dehydrated data). The $AUC_{0\text{-}48\ h}$ ratio of total radiolabeled components over 2′-*O*-methyluridine was ~17, indicating that the parent compound was a minor component of the total radioactivity in dried plasma (fourth most abundant radiolabeled component). Metabolites were separated by UHPLC and subsequently identified using radiodetection and high-resolution accurate mass spectrometry. Ten metabolites (M1-M10) were observed in total. Out of these, the most prominent metabolites in plasma, excreta, and tissues were M1 (uridine), M2 (cytosine), M3 (uracil), and M5 (cytidine) could be structurally identified. For identification of the remaining unknown minor metabolites, a detection issue was encountered, which may be due to a lack of ionization by electrospray, ion suppressions or a *m/z* below 50 Da (lower mass range). Moyer et al. (1985) reported the necessity of applying several chromatographic methods for efficient separation of pyrimidine nucleosides from their nucleotides and metabolites.

Plasma $AUC_{0\text{-}48h}$ for the main metabolites were 32.8% of total radioacitivity AUC, for uridine (M1), 8.11% for cytosine (M2), and 23.6% for uracil (M3), with apparent terminal elimination half-lives of 12.2, 20.3, and 10.0 h for M1, M2, and M3, respectively. All other metabolites

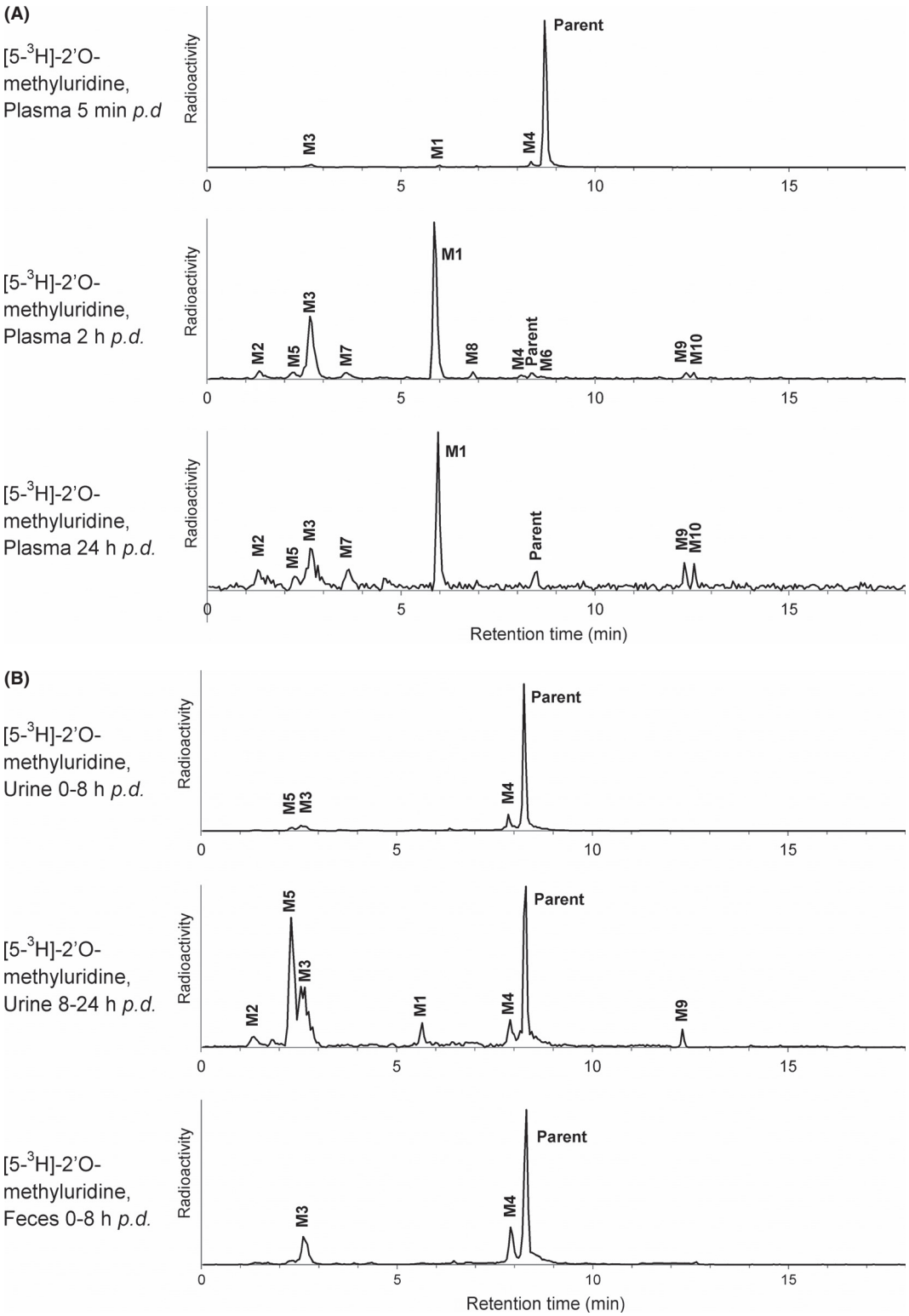

Figure 5. Radiochromatograms of [5-^{3}H]-2′-*O*-methyluridine in excreta and tissues following a single i.v. administration (nominal dose 1 mg/kg). (A) Radiochromatograms of [5-^{3}H]-2′*O*-methyluridine in plasma at 5 min, 2 and 24 h postdose. (B) Radiochromatograms of [5-^{3}H]-2′*O*-methyluridine in urine pooled across the 0–8 h and 8–24 h interval, and feces pooled across the 0–8 h interval. (C) Radiochromatograms of [5-^{3}H]-2′*O*-methyluridine in spleen, lung, salivary gland, small intestine, liver, kidney, and heart at 1 h postdose.

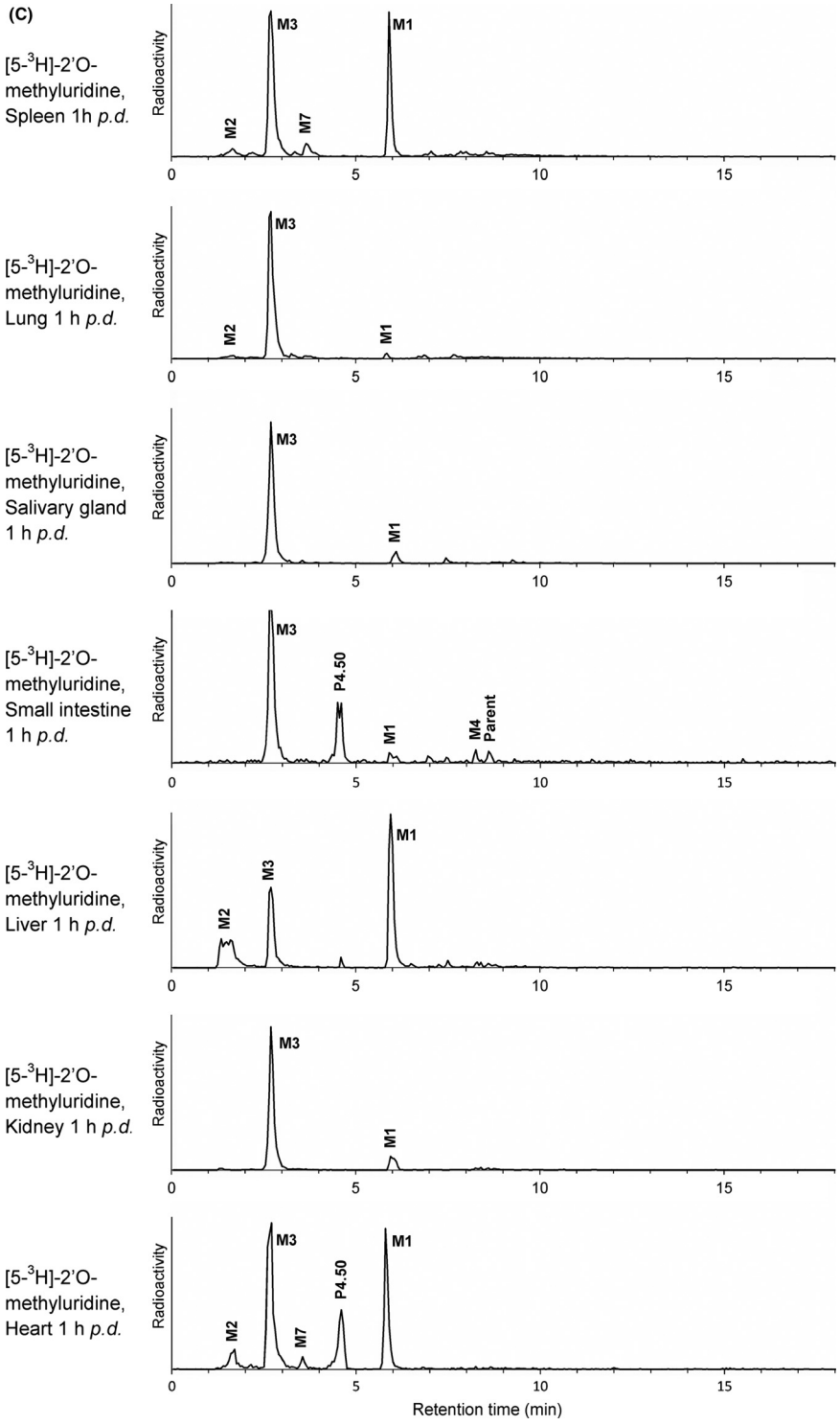

Figure 5.

accounted each for less than 5.2% of $AUC_{0\text{-}48\ h}$. The highest plasma concentrations of uridine and uracil were observed at 30 min after dosing, and were 0.2 and 0.1 μmol/L, respectively. After a single intravenous administration of [5-^{3}H]-2′-*O*-methyluridine, the radioactivity was rapidly and widely distributed throughout the

body, and was determined by QWBA in all tissues investigated up to 48 h after dosing. The radioactivity in all tissues investigated was found to be primarily associated with the metabolites uridine (M1), cytosine (M2), and uracil (M3). Among the investigated tissues, the parent compound was only observed as a minor component in the small intestine. The highest concentrations and exposures of radioactivity were found in the kidney, followed by the spleen, pineal body, and lymph nodes. The exposures of radioactivity (AUC_{last}) in more than 90% of the matrices were greater than that of blood. Total radiolabeled components were detectable in the brain up to 48 h after dosing. Among the investigated tissues, the liver was found to contain the highest percentage of uridine (47.6%). This correlates well with the liver being the major organ responsible for homeostatic control of uridine plasma and tissue concentrations (Yamamoto et al. 2011).

The recovery of radioactivity from urine and feces at 48 h was about 55.1% of the dose, with 45.9% being excreted in urine, 6.81% was in the cage wash, and 2.34% excreted in feces, whereas the remaining radioactivity 38.6% was mainly found in the carcass. These measurements are consistent with the results derived from QWBA, where the highest concentrations of total radiolabeled components were observed in the kidneys. 2′-*O*-methyluridine was rapidly cleared from the plasma compartment and was found to be mainly eliminated via the kidney as intact compound (31.2% of the dose), but also via metabolism (14.7% of the dose). Two of the most prominent metabolites recovered from the urine were uracil (M3) and cytidine (M5), representing 3.61% and 1.83% of the dose, respectively.

The mass balance data showed 38.6% remaining radioactivity in the carcass (at 48 h *p.d.*) which can be explained by the fact that the main metabolites will become part of the endogenous pool of cytidine and uracil. These results are consistent with the salvage pathway of pyrimidines in the kidneys which are recycled from nucleosides, especially uridine (Moyer et al. 1981, 1985; Yamamoto et al. 2011).

The current investigation of the fate of the modified nucleoside provided additional insights into the oligonucleotide disposition. [5-^{3}H]-2′-*O*-methyluridine was the [^{3}H]-nucleotide used in the [^{3}H]-SSB siRNA dosed to male CD-1 mice (both unformulated and formulated, as recently reported Christensen et al. (2013, 2014). 2′*O*Me-modified unformulated [^{3}H]-SSB siRNA was shown to be completely degraded to the radiolabeled nucleoside ([5-^{3}H]-2′-*O*-methyluridine). This nucleoside was further metabolized via an *O*-demethylation to uridine (M1). Metabolite profiling of tissue extracts indicated that the observed tissue distribution of radioactivity (by QWBA) did not reflect intact siRNA or oligonucleotide metabolites, but most likely radiolabeled monomers. Therefore, a head-to-head comparison between the distribution of radioactivity after administration of unformulated [^{3}H]-SSB siRNA and [5-^{3}H]-2′-*O*-methyluridine is appropriate. Precautions should, however, be taken to avoid overinterpretation of the radioactivity data. In both studies, the radioactivity was rapidly and widely distributed throughout the body, and was determined in all tissues investigated up to 48 h after dosing. In both studies, blood concentrations of total radiolabeled components declined slowly, after the initial rapid decline of total radiolabeled components. The concentration-time profiles for tissues were reasonably aligned in both studies, whereas the kidney contained the highest concentration of total radiolabeled components and exposure. The excretion profiles for both studies also correlated well, but with some discrepancies in excreta composition. Overall, this suggests that mouse ADME studies of modified nucleosides could be an attractive and efficient method to discover the fate of unformulated siRNA. The investigation of a monomer [5-^{3}H]-2′*O*-methyluridine and its metabolites in mice indicated that radioactive compounds were excreted via urine (52.7% of dose) by direct excretion of the intact monomer or metabolism. The tritiated water represented 8.67%. The recovery data indicated that notable amounts of compound related radioactivity remained in the body after 48-h postdose. These results were consistent with the QWBA data, and tissue profiles and confirmed that the radioactivity was widely distributed in tissues and in the form of endogenous compounds. [5-^{3}H]-2′*O*-methyluridine was converted to uridine via *O*-demethylation. Subsequently, either a direct *N*-dealkylation of the uridine to the uracil or a phosphorylation process to UTP (uridine triphosphate), followed by CTP (cytidine triphosphate) synthase from UTP, and phosphohydrolyzation to cytidine may have occurred. Uridine kinase may have catalyzed the phosphorylation of uridine to UMP (uridine monophosphate). In the pyrimidine metabolism pathway, UMP's are further phosphorylated by UMP kinase (van Rompay et al. 1999) and nucleoside diphosphate kinases (Parks and Agarwal 1973) to UTP. UTP is then subjected to an amination (Lieberman 1956 or von der Saal et al. 1985) to yield CTP (cytidine triphosphate) followed by a NTP phosphohydrolyzation to CMP (cytidine monophosphate) and a 5′-ribonucleotide phosphohydrolyzation to cytidine. Afterwards, a *N*-dealkylation of the cytidine may occur to produce the cytosine followed by deamination to uracil. As suggested by von der Saal et al. (1985), the formation of phosphorylated uridine followed by extension of cytidine may only be present as intermediate in the overall mechanism. Thus, the reactions depicted in Figure 4 should be considered as possible mechanism as no

intermediate were identified in the scope of this study. Uracil may undergo further metabolism following a reductive or oxidative pathway (Loh et al. 2006). Consequently, we can conclude and assume that that the disposition of the 2′OMe-Uridine will undergo demethylation to uridine and follow the subsequent endogenous pathways.

Acknowledgements

We sincerely thank nonclinical PK/PD for their technical support (Martina Suetterlin, Sandra Wehrle, and Mike Becquet) and to Karine Litherland for her lab support. We would like to extend our thanks to NIBR Analytical Sciences for their NMR support (Lukas Oberer and Thomas Lochmann).

Author Contributions

Participated in research design: Christensen, Faller, van de Kerkhof, Krauser, and Swart.

Conducted experiments: Christensen, Catoire, Garnier, Lozac'h, Faller.

Contributed with new reagents or analytical tools: Christensen, Lozac'h, Faller, van de Kerkhof, Swart, Natt and Hunziker.

Performed data analysis: Christensen, Lozac'h, Faller, van de Kerkhof, Swart.

Wrote or contributed to the writing of the manuscript: Swart, Christensen, Lozac'h, Faller, van de Kerkhof, Krauser.

Disclosures

None declared.

References

Behlke MA (2006). Progress towards in vivo use of SiRNAs. Mol Ther 13: 644–670.

Behlke MA (2008). Chemical modification of SiRNAs for in vivo use. Oligonucleotides 18: 305–319.

Bramsen JB, Kjems J (2011). Chemical modification of small interfering RNA. Methods Mol Biol 721: 77–103.

Castanotto D, Rossi JJ (2009). The promises and pitfalls of RNA-interference-based therapeutics. Nature 457: 426–433.

Chiu YL, Rana TM (2003). SiRNA function in RNAi: a chemical modification analysis. RNA 9: 1034–1048.

Christensen J, Natt F, Hunziker J, Krauser J, Swart P (2012). Tritium labeling of full-lengh small interfering RNAs. J Label Compd Radiopharm 55: 189–196.

Christensen J, Litherland K, Faller T, Van de Kerkhof E, Natt F, Hunziker J, et al. (2013). Metabolism studies of unformulated internally [3H]-labeled SiRNAs in mice. DMD 41: 1211–1219.

Christensen J, Litherland K, Faller F, van de Kerkhof E, Natt F, Hunziker J, et al. (2014). Biodistribution and metabolism studies of LNP-formulated internally [3H]-labeled siRNA in mice. DMD 42: 431–440.

Davies B, Morris T (1993). Physiological-parameters in laboratory-animals and humans. Pharm Res 10: 1093–1095.

Engels JW (2013). Gene silencing by chemically modified SiRNAs. New Biotechnol 30: 302–307.

Lieberman I (1956). Enzymatic amination of uridine triphosphate to cytidine triphosphate. J Biol Chem 222: 765–775.

Loh KD, Gyneshwar P, Markenscoff Papadimitriou E, Fong R, Kim KS, Parales R, et al. (2006). A previously undescribed pathway for pyrimidine catabolism. PNAS 103: 5114–5119.

Morrissey DV, Lockridge JA, Shaw L, Blanchard K, Jensen K, Breen W, et al. (2005). Potent and persistent in vivo anti-HBV activity of chemically modified SiRNAs. Nat Biotechnol 23: 1002–1007.

Moyer JD, Oliver JT, Handschumacher RE (1981). Salvage of circulating pyrimidine nucleosides in the rat. Cancer Res 41: 3010–3017.

Moyer JD, Malinowski N, Ayers O (1985). Salvage of circulating pyrimidine nucleosides by tissues of the mouse. J Biol Chem 260: 2812–2818.

Parks RE, Agarwal RP (1973). Nucleoside diphosphokinases. Pp. 307–334 *in* P. D. Boyer, ed. The Enzymes. Academic Press, New York.

Rana TM (2007). Illuminating the silence: understanding the structure and function of small RNAs. Nat Rev Mol Cell Biol 8: 23–36.

Rasenack J, Nowack J, Decker K (1978). Pyrimidine nucleotide biosynthesis and turnover in rat skeletal muscle and liver. Eur J Biochem 88: 475–482.

Richardson FC, Tennant BC, Meyer DJ, Richardson KA, Mann PC, Mcginty GR, et al. (1999). An evaluation of the toxicities of 2′ -fluorouridine and 2′-fluorocytidine-HCl in F344 rats and woodchucks (marmota monax). Toxicol Pathol 27: 607–617.

Richardson FC, Zhang C, Lehrman SR, Koc H, Swenberg JA, Richardson KA, et al. (2002). Quantification of 2′-Fluoro-2′-deoxyuridine and 2′-fluoro-2′-deoxycytidine in DNA and RNA isolated from rats and woodchucks using LC/MS/MS. Chem Res Toxicol 15: 922–926.

Richmond CR, Langham WH, Trujillo TT (1962). Comparative metabolism of tritiated water by mammals. J Cell Compara Physiol 59: 45–53.

van Rompay AR, Johansson M, Karlsson A (1999). Phosphorylation of deoxycitidine analog monophosphates by UMP-CMP kinase: molecular characterization of the human enzyme. Mol Pharmcol 56: 562–569.

von der Saal W, Anderson PM, Villafrance JJ (1985). Mechanistic investigations of *Eschericia coli* cytidine-5′-triphosphate synthetase. J Biol Chem 260: 14993–14997.

Shukla S, Sumaria CS, Pradeepkumar PI (2010). Exploring chemical modifications for SiRNA therapeutics: a structural and functional outlook. Chem Med Chem 5: 328–349.

Singh S, Narang A, Mahato R (2011). Subcellular fate and off-target effects of SiRNA, ShRNA, and MiRNA. Pharm Res 28: 2996–3015.

Smith CM, Steitz JA (1997). Sno storm in the nucleolus: new roles for myriad small RNPs. Cell 89: 669–672.

Tse F, Jaffe JM (1991). Preclinical drug disposition. Marcel Decker Inc, New York, NY.

Watts JK, Deleavey GF, Damha MJ (2008). Chemically modified SiRNA: tools and applications. Drug Discov Today 13: 842–855.

Werner M, Purta E, Kaminska KH, Cymerman IA, Campbell DA, Mittra B, et al. (2011). 2′-O-ribose methylation of Cap2 in human: function and evolution in a horizontally mobile family. Nucl Acids Res 39: 4756–4768.

Whitehead KA, Langer R, Anderson DG (2009). Knocking down barriers: advances in SiRNA delivery. Nat Rev Drug Discov 8: 129–138.

Yamamoto T, Koyama H, Kurajoh M, Shoji T, Tsutsumi Z, Moriwaki Y (2011). Biochemistry of uridine in plasma. Clin Chim Acta 412: 1712–1724.